

# Glycosphingolipid Synthesis in Cerebellar Purkinje Neurons: Roles in Myelin Formation and Axonal Homeostasis

## GLIA

### Glycosphingolipid Synthesis in Cerebellar Purkinje Neurons: Roles in Myelin Formation and Axonal Homeostasis

SHUN MATSUNAGA,<sup>1,2</sup> OHROU ENDO,<sup>1</sup> KEIICHI ITOHARA,<sup>1</sup> TOMOHIRO HOSHI,<sup>1,2</sup> HIROYUKI HIGASHI,<sup>1</sup> KAZUYUKI YAMADA,<sup>1</sup> NAOKIYO TORIYAMA,<sup>1</sup> YOSHIO YAMAMOTO,<sup>1</sup> AND YASUHIRO HIRAHARA<sup>1,2</sup>  
<sup>1</sup>Department of Molecular, Cellular, and Integrative Neuroscience, Brain Science Institute, RIKEN, Wako, Saitama, Japan  
<sup>2</sup>Department of Neurobiology, Faculty of Life Sciences, University of Tsukuba, Tsukuba, Ibaraki, Japan

スフィンゴ糖脂質は、脳組織に豊富に含まれており、発達に伴いその量、質ともに変化する。そのため、古くから神経系における機能が注目されており、発達における神経突起伸長、神経伝達などの神経機能への関与が示唆されてきた。近年では、さらに各種のスフィンゴ糖脂質合成酵素ノックアウトマウスを用いて個体レベルでの機能解析がなされている。多くのスフィンゴ糖脂質は、グルコシルセラミドを出発物質として合成されるため、グルコシルセラミドを合成するUDP-グルコースセラミドグルコシルトランスフェラーゼ(Ugcg、もしくはGlcT-1)はガングリオシド代謝全体をコントロールする重要な酵素である。実際に、GlcT-1ノックアウトマウスは発生初期に死亡し、個体レベルにおいてきわめて重要な機能を担っていると考えられる。しかしながら、胎生初期に致死であるため神経細胞におけるGlcT-1の機能は明らかとはならなかった。そこで、我々は、小脳皮質神経細胞の一種であるプルキンエ細胞特異的にGlcT-1遺伝子を欠損したマウスを、Cre/loxPシステムにより作製し、GlcT-1欠損が神経細胞に及ぼす影響を解析した。このマウスでは、プルキンエ細胞がほぼ成熟した後、Creが発現することから、成熟した神経細胞における影響を主に解析できる。このマウスのプルキンエ細胞の形態を観察したところ、軸索に顕著な形態異常が認められた。すなわち、プルキンエ細胞の軸索は膨大した形態を示し、軸索輸送される積荷タンパク質の貯留が認められた。さらに、ミエリンの形態も異常を示し、軸索とオリゴドendロサイト間の細胞間相互作用に軸索側のスフィンゴ糖脂質が重要であることが示唆された。

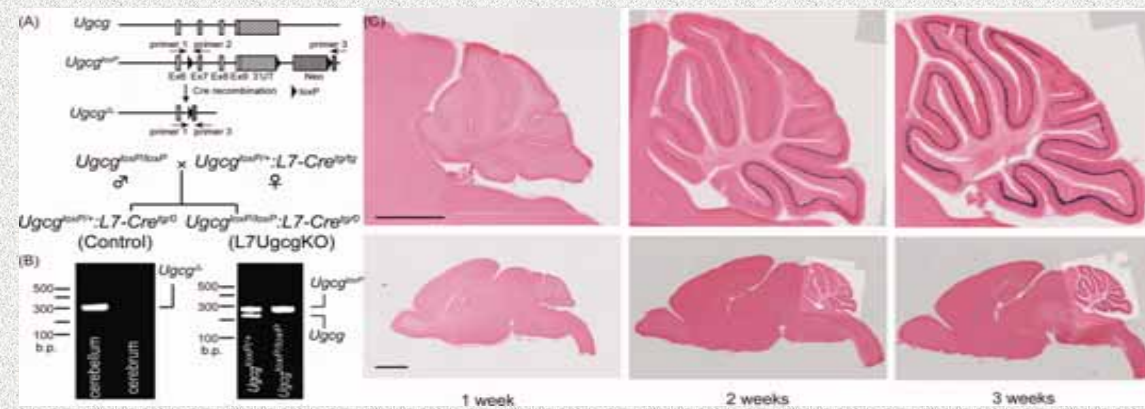


Fig. 1. Generation and characterization of floxed allele. A: Schematic representation of Cre-mediated recombination of UgcgloxP. The predicted outcome of Cre recombination is shown at the bottom. B: Identification of the UgcgloxP allele in brain (left panel). Genomic DNA from cerebellum and cerebrum of 8-week-old L7UgcgKO mice were subjected to PCR analysis using primers 1 and 3. Identification of the UgcgloxP allele (right panel). Tail DNA from UgcgloxP/1: L7-Cre<sup>tg</sup>/0 and UgcgloxP/loxP: L7-Cre<sup>tg</sup>/0 mice were subjected to PCR analysis using primers 1 and 2. C: An L7-Cre mouse was bred with a Rosa26-lacZ reporter mouse, and Cre expression in the cerebellum of the resulting progeny was assessed for b-galactosidase activity. In the sagittal sections from mice 1–3 postnatal weeks old, blue-colored staining indicates Purkinje cell-specific Cre expression. Scale bars: 2 mm (lower panels); 1 mm (upper panels).

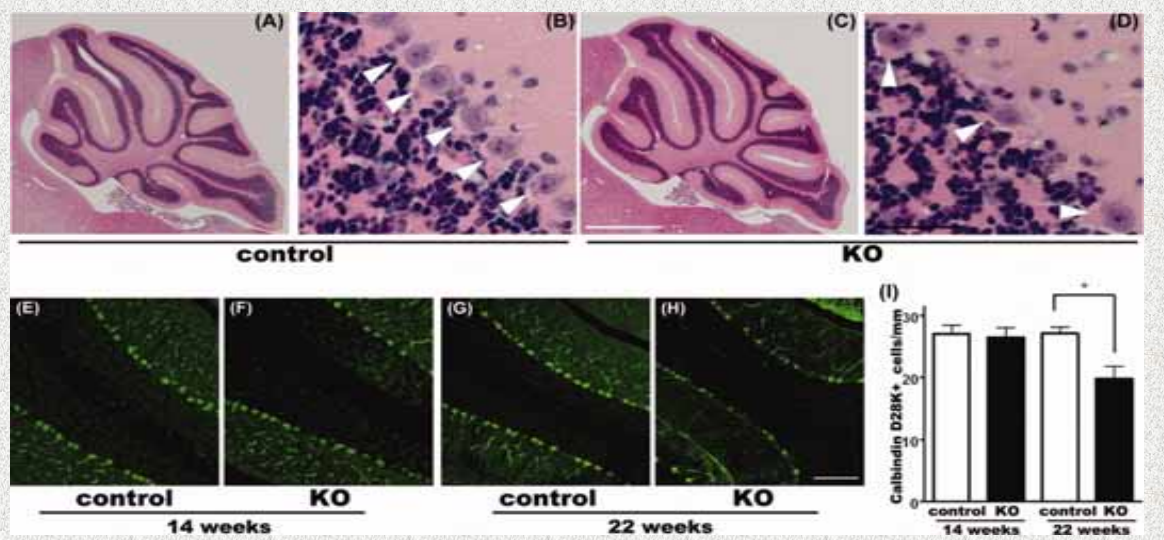
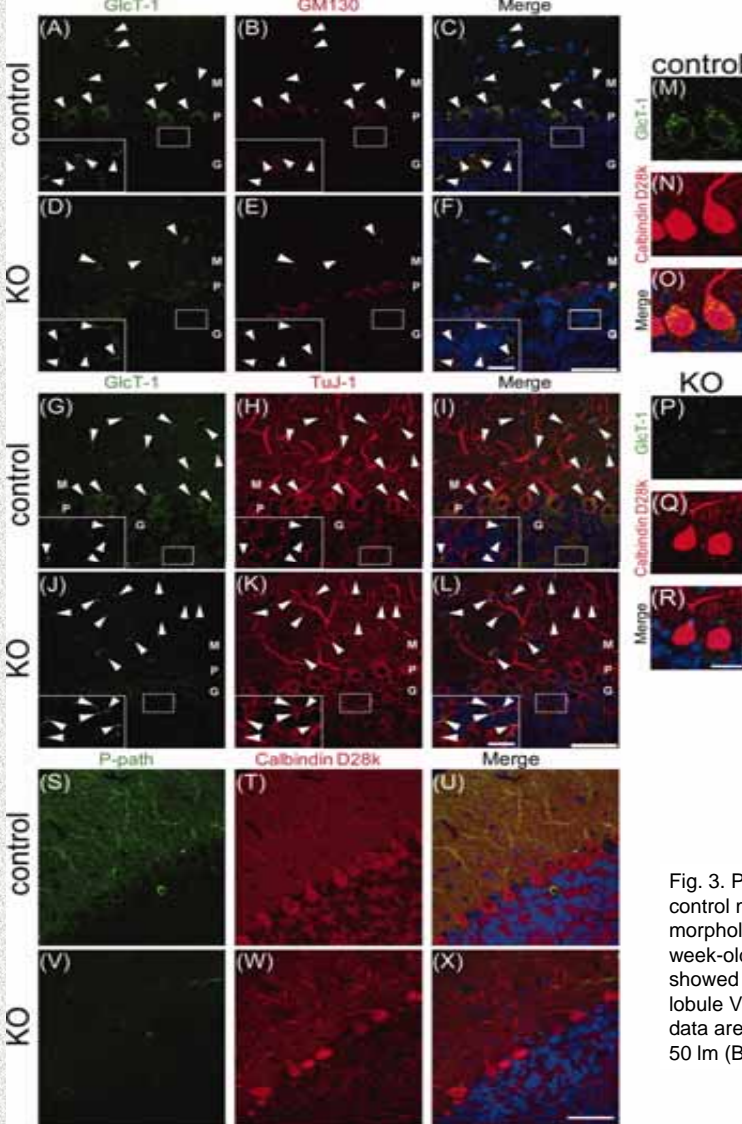


Fig. 2. Deletion of glucosylceramide synthase (GlcT-1) and an anabolite of glucosylceramide, O-acetyl GD3 (P-path antigen), were confirmed in eight-week-old Purkinje cell-specific Ugcg KO mice. A–F: Anti-GlcT-1 (A, D); anti-GM130 (Golgi apparatus marker, B, E); and merged (C, F). G–L: Anti-GlcT-1 (G, J); anti-TuJ-1 (neuronal marker, H, K); and merged (I, L). M–R: Anti-GlcT-1 (M, P); anti-calbindin D28k (N, Q); and merged (O, R). S–X: P-path (S, V); anti-calbindin D28k (T, W); and merged (U, X). Insets show high magnification images of the white rectangular area in the granular layer. In the merged micrographs, cell nuclei were visualized with DAPI staining (blue). M, molecular layer; P, Purkinje cell layer; G, granule cell layer. Arrowheads point to GlcT-1-immunopositive cells. These results were observed in all mice of each genotype (n 5 3). Scale bars: 50  $\mu$ m (A–L, S–X); 20  $\mu$ m (M–R); 10  $\mu$ m (insets).

Fig. 3. Purkinje cell loss in L7UgcgKO mice. A–D: Hematoxylin and eosin (H&E)-stained cerebellar sections from 22-week-old control mice (A, B) and KO mice (C, D). Mid-sagittal sections through the entire extent of the cerebellum (A, C) show intact morphology in KO mice. Arrowheads point to Purkinje cell somata (B, D). Cerebellar sections from 14-week-old (E, F) and 22-week-old (G, H) control and KO mice were immunostained with anti-calbindin D28k, a Purkinje cell marker. L7UgcgKO mice showed Purkinje cell loss at 22 weeks (H), but no significant Purkinje cell loss at 14 weeks (F). Quantitation of Purkinje cells in lobule V of midsagittal sections of control and L7UgcgKO mice at 14 and 22 weeks; anti-calbindin D28k stained Purkinje cells. The data are expressed as number of Purkinje cells per millimeter of Purkinje cell layer; n 5 3, \*P < 0.05 (I). Scale bars: 1 mm (A, C); 50  $\mu$ m (B, D); 100  $\mu$ m (E–H).

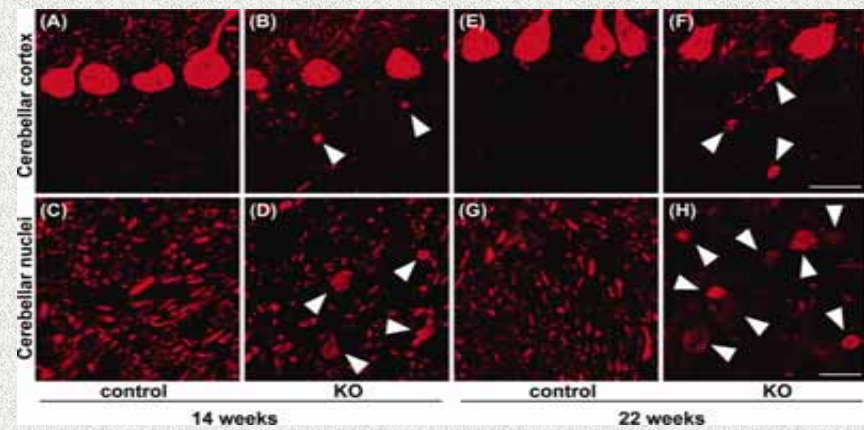


Fig. 4. Axonal swellings of Purkinje cells in L7UgcgKO mice. Cerebellar sections from 14-week-old and 22-week-old control and KO mice were immunostained with anti-calbindin D28k antibody. After postnatal week 14, axonal swellings were observed in both cerebellar deep nuclei (D, 14 weeks; H, 22 weeks) and cerebellar cortex (B, 14 weeks; F, 22 weeks). Control mice showed no axonal dystrophy in cerebellar cortex (A, 14 weeks; E, 22 weeks) or deep cerebellar nuclei (C, 14 weeks; G, 22 weeks). Arrowheads indicate axonal swellings. Scale bars: 25  $\mu$ m for cerebellar cortex; 10  $\mu$ m for cerebellar nuclei.

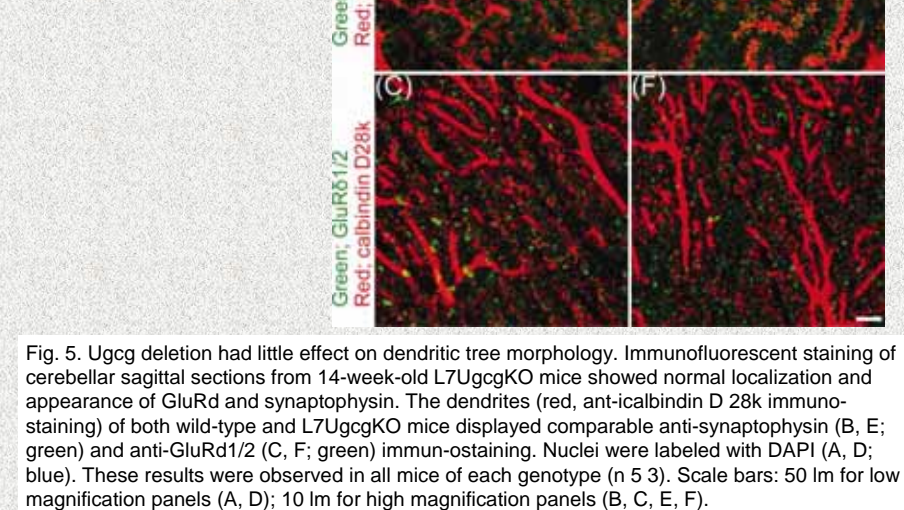


Fig. 5. Ugcg deletion had little effect on dendritic tree morphology. Immunofluorescent staining of cerebellar sagittal sections from 14-week-old L7UgcgKO mice showed normal localization and appearance of GluR $\delta$  and synaptophysin. The dendrites (red, anti-calbindin D28k immunostaining) of both wild-type and L7UgcgKO mice displayed comparable anti-synaptophysin (B, E; green) and anti-GluR $\delta$ 1/2 (C, F; green) immunostaining. Nuclei were labeled with DAPI (A, D; blue). These results were observed in all mice of each genotype (n 5 3). Scale bars: 50  $\mu$ m for low magnification panels (A, D); 10  $\mu$ m for high magnification panels (B, C, E, F).

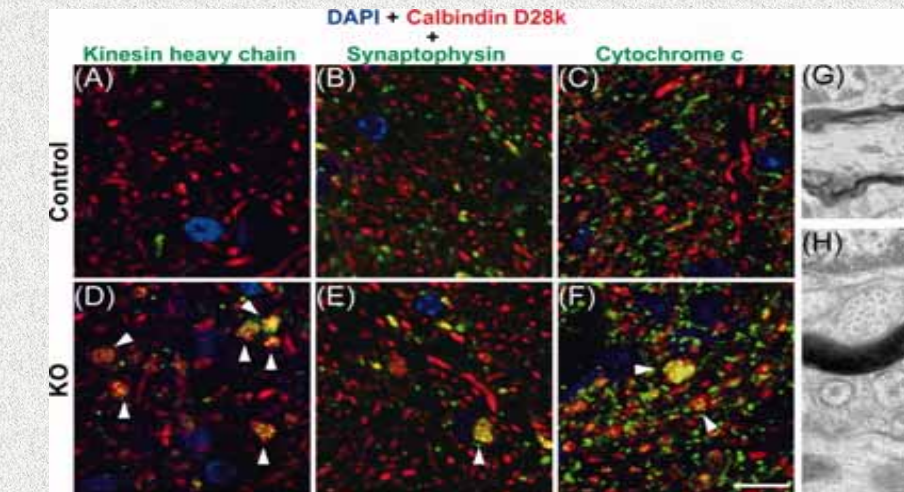


Fig. 6. Intense staining for mitochondria, synaptic vesicles, and kinesin heavy chain were observed in axonal swellings, suggesting that axonal transport was severely defective in L7UgcgKO mice. Cerebellar sections were co-immunostained with anti-calbindin D28k (red) and antibodies against cargo markers (green), such as anti-kinesin heavy chain (A, D); anti-synaptophysin (B, E); or anti-cytochrome c (C, F). Nuclei were labeled with DAPI (blue). Arrowheads indicate axonal swellings. Scale bar: 10  $\mu$ m (A–F). Transmission electron micrograph showing the ultrastructure of a swollen axon from a L7UgcgKO mouse (G, H). Aberrant membrane structures and mitochondria accumulated within axonal swellings. These results were observed in all mice of each genotype (n 5 3). Scale bars: 1  $\mu$ m (G); 0.3  $\mu$ m (H).

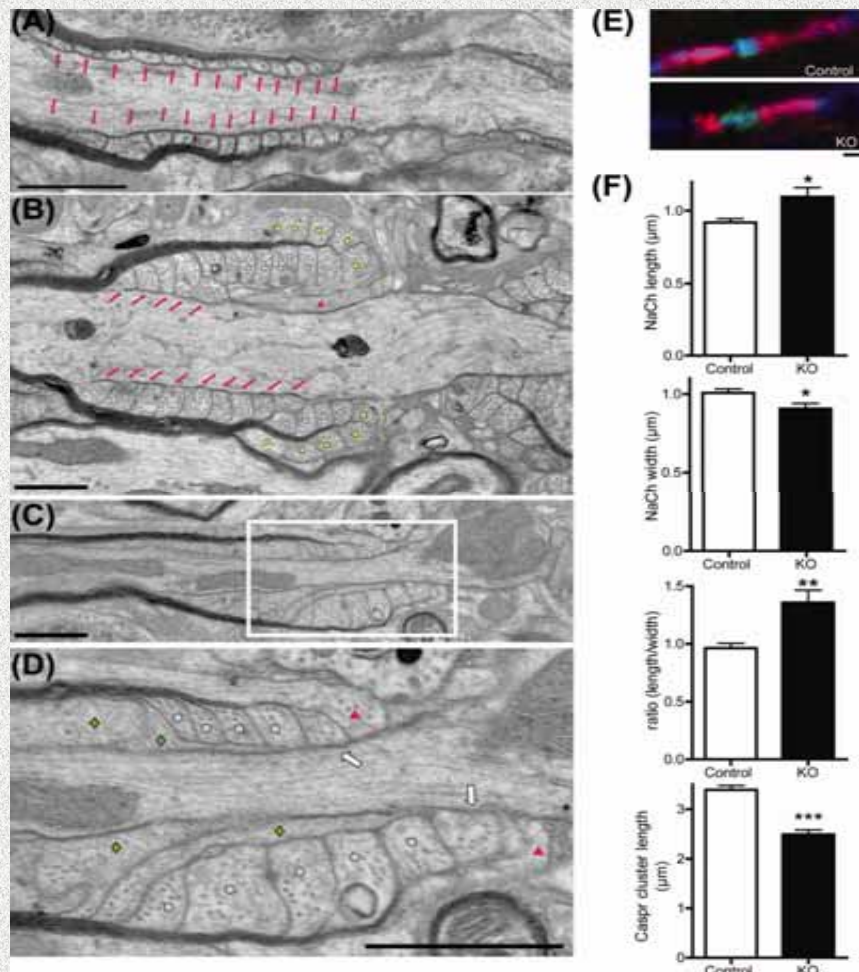


Fig. 7. L7UgcgKO mice exhibit ultrastructural abnormalities at paranodes. Longitudinal section through the paranodal portion of an axon from a control mouse (A) and KO mice (B–D). A: Normal ultrastructure of node and paranode of a control mouse. The cytoplasmic loops at the paranode are arranged orderly and are attached to the axolemma with a transverse band (TB, red arrow), indicating that at the paranode, the axon is enveloped by oligodendrocyte loops with a continuous TB. B: Abnormal paranode from a 22-week-old L7UgcgKO mouse. A compact myelin sheath consisting of 18 lamellae wraps this axon. Of the 18 lamellae, nine of the lower and five of the upper paranodal cytoplasmic loops attach themselves onto the axolemma with TB (red arrows). The remaining loops, however, show abnormal contact with the axolemma (circles). The number of lower paranodal cytoplasmic loops contacting the axolemma with a TB is greater than that of the upper loops: nine vs. five normal loops, respectively. This indicates that TBs distribute discontinuously. Some loops (yellow circles) face away from the axon, presumably due to cytoplasmic loop abnormalities. A glial process (red triangle), presumably from an astrocyte, invades the space between the paranodal loops of the oligodendrocyte and axolemma. C: Abnormal paranode from a 14-week-old KO mouse. D: High-magnification image of the white rectangular area in (C). Two paranodal loops (white arrows) directly contact the axolemma. Other paranodal loops (blue circles), however, do not directly contact the axolemma. Deformed loops (green diamonds) attach to the axolemma without TBs. These structures indicate abnormal arrangement of paranodal cytoplasmic loops. These results were observed in all mice of each genotype (n 5 3). Red triangles indicate processes that are presumably from an astrocyte. E: Cerebellar sections were co-immunostained with anti-IP3R1 (blue), anti-Caspr (red), and anti-pan sodium channel (green) antibodies. Elongated sodium channel clusters and shorter Caspr clusters were observed in L7UgcgKO mice. F: Quantitation of sodium channel cluster length, width, length-to-width ratio, and Caspr cluster length in lobule V of midsagittal sections of 17- to 22-week-old control and L7UgcgKO mice (n 5 3). \*P < 0.05; \*\*P < 0.01; \*\*\*P < 0.001 compared with control mice. Scale bar: 1  $\mu$ m (A–E).

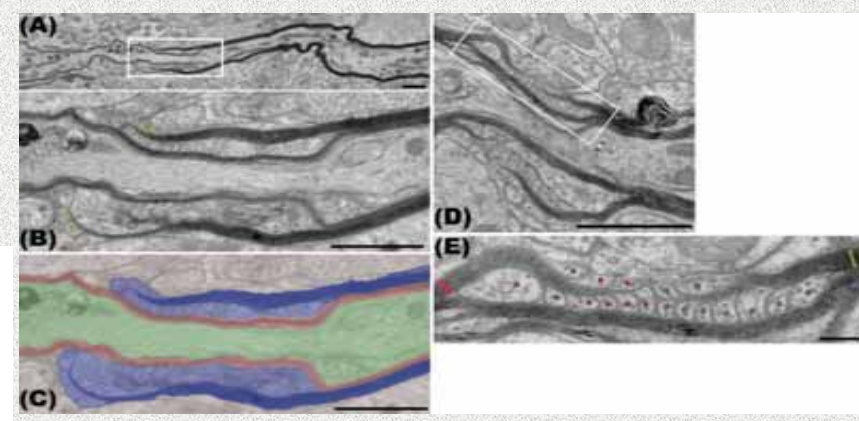


Fig. 8. Longitudinal section through axons from L7UgcgKO mice showing concentric, excessive myelin sheath formation with paranodelike structure. A: Doubly myelinated and hemiparanode-like structure from a 14-week-old KO mouse. B: High-magnification electron micrograph of the white rectangular area in Panel A. Myelin lamellae of outer myelin sheaths (dark blue, Panel C) terminate with cytoplasm filled paranode-like loops (circles in this panel; light blue, Panel C) on inner myelin sheaths (red, Panel C). D: Excessive paranode-like loops from a 22-week-old KO mouse. E: High-magnification electron micrograph of the white rectangular area in Panel D. On the left-hand side bilateral paranodal loop-like structures filled with cytoplasm marked with red circles are derived from nine-layered myelin lamellae (red bar); those marked with green circles are from nine-layered myelin lamellae coming from the right-hand side (green bar). These paranodal-like loops attach onto the inner compact myelin sheaths, i.e., the original myelin sheath. This symmetrical arrangement of loops is similar to that at the node of Ranvier. These results were observed in all mice of each genotype (n 5 3). Scale bars: 1  $\mu$ m (A–C); 0.5  $\mu$ m (D, E).

**結語**  
 プルキンエ細胞特異的GlcT-1欠損マウスの解析を通じて、成熟した神経細胞のスフィンゴ糖脂質は軸索の形態維持に重要であるばかりでなく、ミエリン形成に関わるグリア細胞の正常な機能維持にも重要な役割を果たしていることが明らかとなった。